Marine Geology 277 (2010) 21–30

Contents lists available at ScienceDirect

Marine Geology

journal homepage: www.elsevier.com/locate/margeo

Chemical environment of cold seep carbonate formation on the northern continental slope of South China Sea: Evidence from trace and rare earth element geochemistry

Lu Ge [a,b], Shao-Yong Jiang [a,*], Rudy Swennen [b], Tao Yang [a], Jing-Hong Yang [a], Neng-You Wu [c], Jian Liu [c], Dao-Hua Chen [c]

[a] State Key Laboratory for Mineral Deposits Research, Department of Earth Sciences, Nanjing University, Nanjing 210093, China
[b] Department of Earth and Environment Sciences, Geology, K.U.Leuven, B-3001 Heverlee, Leuven, Belgium
[c] Guangzhou Marine Geological Survey, Guangzhou 510760, China

ARTICLE INFO

Article history:
Received 1 August 2009
Received in revised form 12 July 2010
Accepted 6 August 2010
Available online 15 August 2010

Communicated by G.J. de Lange

Keywords:
rare earth elements (REE)
Ce anomaly
redox condition
cold seep carbonates
South China Sea

ABSTRACT

Trace element and rare earth element (REE) concentrations in cold seep carbonates from the northern continental slope of the South China Sea are used in this study to indicate source fluid characteristics and redox conditions. Carbonate samples from the two study areas (Shenhu and Dongsha) all show low total REE concentrations (mostly 10–20 ppm). In the Shenhu area, the shale-normalized REE patterns of the chimney carbonates display slight light REE enrichment, positive Ce anomaly, and a consistently positive Gd anomaly. These carbonate chimneys show a two-stage formation history, with a slight increase in the positive Ce anomaly from the rim to core. Trace and rare earth element data suggest that the core may have formed in a more anoxic condition than the rim. In the Dongsha area, seep carbonate samples show a slight heavy REE enrichment, with both negative and positive Ce anomalies, and more positive Gd anomalies, which are consistent with precipitation in an anoxic environment. Redox sensitive trace elements, such as Mo, U, Ni, V and Co, also indicate anoxic conditions for this cold seep carbonate precipitation.

1. Introduction

Methane-derived carbonate precipitation is a well known phenomenon at hydrocarbon seeps on active and passive continental margins worldwide (Bohrmann et al., 1998; Peckmann et al., 2001; Campbell et al., 2002; Peckmann and Thiel, 2004). At cold seep sites, methane serves as an energy source for microbial communities (LaRock et al., 1994; Hinrichs et al., 1999), and seep carbonates are products of the microbial oxidation of methane (Peckmann et al., 1999). The methane oxidation reaction can take place using both aerobic and anaerobic processes (Canet et al., 2003). In the case of anaerobic oxidation of methane, a microbial community consisting of methane-oxidizing archaea and sulfate-reducing bacteria consumes sulfate and methane in a 1:1 molar ratio (Reeburgh, 1976; Hinrichs et al., 1999). Anaerobic oxidation produces sulfide and bicarbonate (HCO_3^-), which leads to an increase in alkalinity that favors carbonate precipitation (Ritger et al., 1987; Paull et al., 1992; Peckmann et al., 2001). On the other hand, aerobic methane oxidation produces CO_2, decreasing pH, and potentially inducing the dissolution of carbonates (Wallmann et al., 1997). However, aerobic methane oxidation plays a minor role compared to anaerobic oxidation, as bottom water oxygen, with concentrations lower than 200 mmol/L at seep and methane-rich sites, is often limited to the uppermost few millimeters of the sediment (Kruger et al., 2005) and therefore is available in much lower concentrations when compared to sulfate (28.9 mmol/L, D'Hondt et al., 2002).

Trace and rare earth element (REE) concentrations recorded in chemical sediments have been used to obtain information on marine environments and the fluids from which these rocks originate (Wright et al., 1987; Frimmel, 2009). It is well known that geochemical properties of REE are powerful tracers of chemical processes in the marine environment (Haley et al., 2004). The distribution of these elements is very sensitive to water depth, salinity and oxygen level (Frimmel, 2009). Anomalies in the contents of the redox-sensitive elements, such as Ce, provide information on oceanic oxygenation. No fractionation of Ce occurs under reducing conditions, resulting in Ce concentrations from normal to enriched in anoxic environments (Webb and Kamber, 2000; Frimmel, 2009).

The REE characteristics have been extensively discussed, both for hydrothermal carbonate deposits and modern marine carbonates. Their concentrations, shale-normalized REE patterns, and Ce and Eu anomalies in carbonates provide information of oceanic redox environments (Sarkar et al., 2003; Frimmel, 2009). However, geochemical properties of cold seep carbonates have seen limited attention regarding their REE patterns, with only a few data reported from settings in the northern

* Corresponding author.
E-mail address: shyjiang@nju.edu.cn (S.-Y. Jiang).

0025-3227/$ – see front matter © 2010 Elsevier B.V. All rights reserved.
doi:10.1016/j.margeo.2010.08.008

South China Sea, Gulf of Mexico, and Black Sea (Chen et al., 2005; Feng and Chen, 2008; Feng et al., 2009a,b; Feng et al., 2010). Variable contents of trace elements, total REE, and Ce anomalies in those studied cold seep carbonates have reflected the variable and complex formation conditions.

In this paper, we report on the trace element and REE geochemical characteristics of cold seep carbonates in two locations (i.e., Shenhu and Dongsha) from the northern continental slope of the South China Sea. Since REE patterns are just beginning to be used as an archive of formation conditions of seep carbonates, hence our study, focused on the REE contents, REE distribution patterns, and Ce and Eu anomalies, together with selected redox-sensitive trace elements, will improve our understanding of the applicability of these geochemical tools for the reconstruction of palaeocean environments.

2. Geologic setting

The South China Sea is located at the junction of three plates, the Eurasian, Pacific and Indo-Australian plates. It is underlain by oceanic basement populated with volcanic structures, which presently are filled with sediments, and several of the volcanic structures have developed deep-reaching faults forming fluid pathways (Han et al., 2008). Hence, the northern margin, which has a high sedimentation rate, contains faulted terraces and basins providing significant sources of oil and natural gas, and is considered as a favorable place for gas hydrate formation and accumulation (Shyu et al., 1998; Jin and Wang, 2002; McDonnell et al., 2002; Jiang et al., 2004). Our study area is located in the northern passive margin of the South China Sea, where gas hydrates were firstly drilled in the Shenhu area at 153–225 m below the seafloor in 2007 (Zhang et al., 2007).

In 2004, a cruise of the research vessel Haiyangsihao trawled carbonate chimneys in the Shenhu area (Fig. 1), which is adjacent to several large oil and gas fields with thick sediments rich in organic matter (TOC = 0.44 wt.%–1.75 wt.%) and an unusually high concentration of methane (Lu et al., 2006; Wu et al., 2006). In the same year, the joint Chinese–German RV Sonne Cruise 177 discovered cold seep carbonates in the NE part of the Dongsha area (Fig. 1), which is at the transition between the passive northern margin and the accretionary eastern margin off SW Taiwan Island (Suess, 2005; Han et al., 2008).

3. Samples and methods

Five samples from Shenhu (SH) and nine samples from Dongsha (DS) were collected during the two above-mentioned cruises. Shenhu samples contain a whole chimney and four chimney fragments (Fig. 2A; Table 1). The biggest chimney is about 11 cm long and 6 cm in diameter. Obvious conduits occur in the center of the chimney, with layered structures likely due to multiple stages of seepage. A hash of different fossils, such as foraminifera, is found on the surface of the chimney. The chimneys are composed of variable contents of high Mg calcite (HMC), low Mg calcite (LMC), aragonite, dolomite, clay minerals and terrigenous quartz and feldspar (Table 2). Carbonates from three sites (HS4DG-1, HS4DG-2 and HS4DG-3) show a slightly different mineral composition. HS4DG-1 chimneys mainly consist of

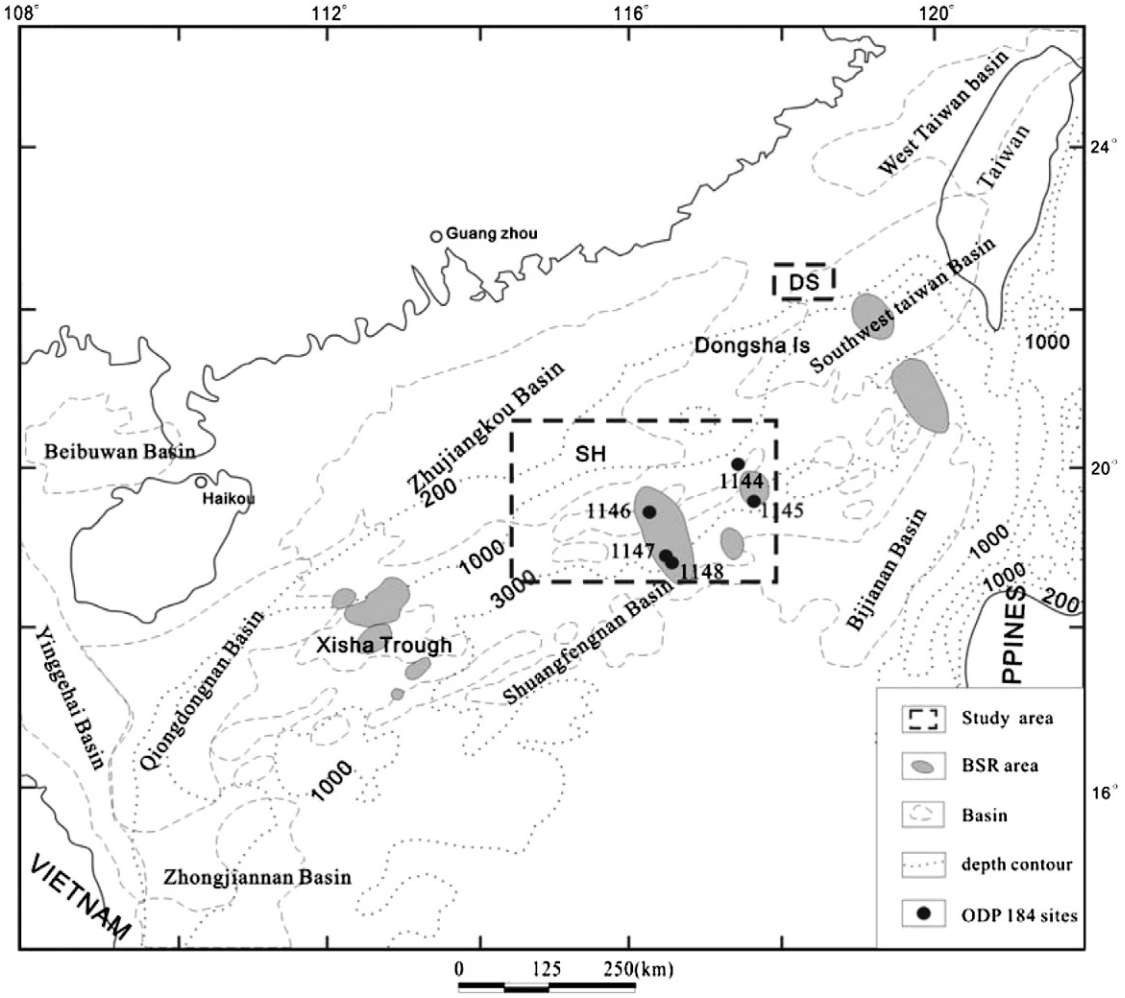

Fig. 1. Location of the study areas on the northern continental slope of South China Sea. SH: Shenhu area, DS: Dongsha area.

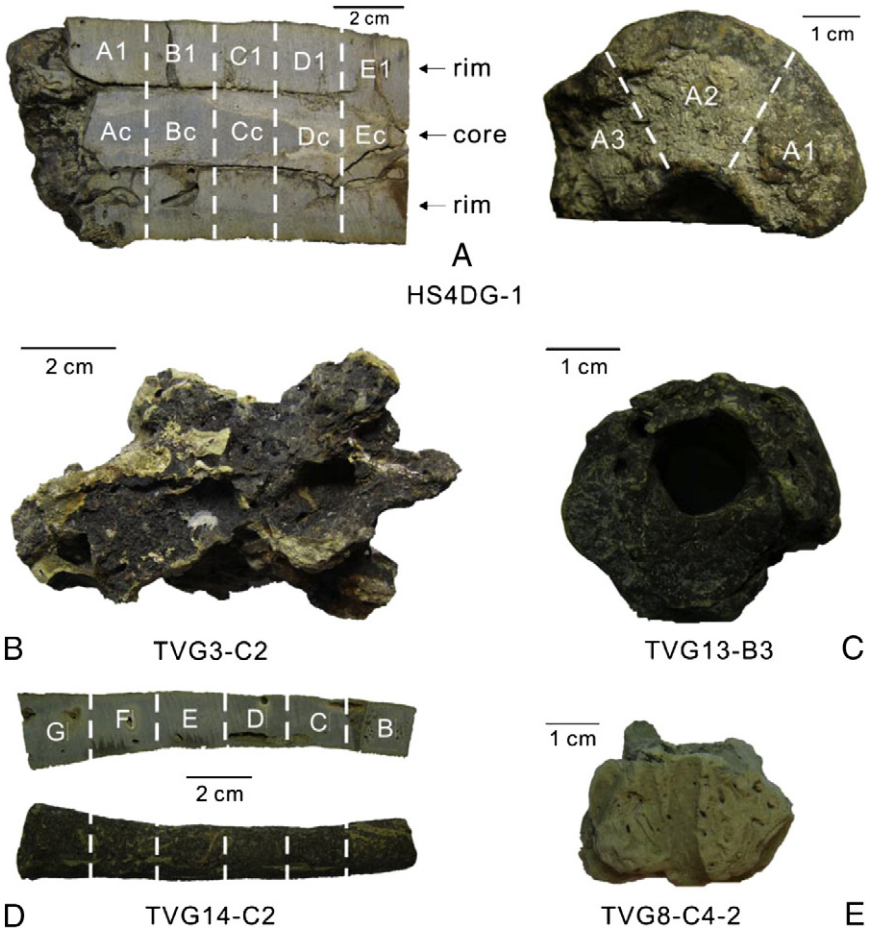

Fig. 2. Typical morphologies of the Shenhu and Dongsha cold seep carbonates. A is from the Shenhu area while the other samples are from the Dongsha area. (A) Chimney with abundant bioclasts (foraminifera, bivalves and gastropods); A1 to E1 represent the rims and Ac to Ec represent the cores. The right picture is the cross-transect of the left chimney. (B) Irregular porous crust from Dongsha-site 1. (C) Thick columnar chimney from Dongsha-site 2. (D) Slender tubular concretion from Dongsha-site 2. (E) Concretion from Dongsha-site 3.

dolomite, while samples from HS4DG-2 contain dolomite and HMC, and aragonite is the dominant mineral in the HS4DG-3 site sample.

Seep carbonates from the Dongsha (DS) area were sampled at three sites (Table 1). These samples are scattered on the seafloor or protruded from the sediments. Site 1 is the shallowest site, with water depths between 473 and 498 m. Samples are comprised of tubes, blocks, cemented burrows, and doughnut/irregular-shaped concretions (Fig. 2B). Carbonate chimneys and chimney fragments are common at site 2 (Fig. 2C, D). Site 3, named as Jiulong Methane Reef at ~760 m water depth (Suess, 2005), consists of a chemoherm buildup about 30 m high and 100 m in diameter above the base. Samples collected at site 3 are mainly green–gray irregular concretions and crusts (Fig. 2E). Mineralogically, except TVG1 and TVG3-C2, high Mg calcite (HMC) is the dominant composition of the Dongsha samples (Table 2). Other carbonate minerals (LMC, aragonite and dolomite), clay minerals and detrital quartz and feldspar also occur in the Dongsha carbonates.

Table 1
Location and description of cold seep carbonates from the Shenhu and Dongsha areas.

Location	Depth (m)	Sample code	Description
Shenhu			
HS4DG			
		HS4DG-1	Chimney
		HS4DG-2A	Chimney fragment
		HS4DG-2B	Chimney fragment
		HS4DG-3A	Chimney fragment
		HS4DG-3B	Chimney fragment
Dongsha-Site 1			
TVG1	498	TVG1	Chimney fragment
TVG2	484	TVG2-C2	Crust
TVG3	473	TVG3-C2	Crust
Dongsha-Site 2			
TVG13	555	TVG13-B3	Chimney
TVG14	533	TVG14-C2	Tube
Dongsha-Site 3			
TVG6	769	TVG6	Concretion
TVG8	769	TVG8-C1	Concretion
		TVG8-C4-2	Concretion
TVG11	769	TVG11-C2	Concretion

Table 2
Mineral compositions of seep carbonates from the Shenhu and Dongsha areas.

Sample code	Major	Minor	Trace
HS4DG-1	Dol	HMC, Qz, Clay	LMC, Ara, fsp
HS4DG-2B	Dol, HMC	Qz, Clay	LMC, Ara, fsp
HS4DG-3B	Ara	HMC, Qz, Clay	LMC, Dol, fsp
TVG1	LMC	HMC, Qz, Clay	Dol, fsp
TVG2-C2	HMC	Qz, Clay	LMC, Dol, fsp
TVG3-C2	Ara	Qz, Clay	LMC, HMC, fsp
TVG6	HMC	Qz, Clay	LMC, Ara, Dol, fsp
TVG8-C4-2	HMC	Qz, Clay	LMC, Ara, Dol, fsp
TVG11-C2	HMC	Clay	LMC, Ara, Dol, Qz, fsp
TVG14-C2	HMC	Qz, Clay	LMC, Dol, fsp

Mineral abbreviation: LMC = low-Mg calcite, HMC = high-Mg calcite, Ara = aragonite, Dol = dolomite, Qz = quartz, fsp = feldspar, Clay = clay minerals.

Table 3
REE concentrations (in ppm) for the Shenhu cold seep carbonates.

	HS4DG-1-A1	HS4DG-1-A2	HS4DG-1-A3	HS4DG-1-Ac	HS4DG-1-B1	HS4DG-1-Bc	HS4DG-1-C1	HS4DG-1-Cc	HS4DG-1-D1	HS4DG-1-Dc	HS4DG-1-E1	HS4DG-1-Ec	HS4DG-2-A	HS4DG-2-B	HS4DG-3-A	HS4DG-3-B
La	2.46	2.54	2.67	1.95	2.54	2.18	2.59	1.91	2.81	1.96	2.91	2.01	3.46	3.20	5.51	4.38
Ce	5.68	5.84	6.57	4.92	6.13	5.35	6.08	4.49	6.35	4.87	6.42	3.83	7.03	7.12	4.60	4.36
Pr	0.60	0.59	0.67	0.48	0.64	0.52	0.65	0.46	0.66	0.48	0.67	0.47	0.76	0.72	1.21	0.94
Nd	2.29	2.27	2.54	1.77	2.49	2.02	2.51	1.78	2.56	1.80	2.52	1.85	3.12	2.82	4.69	3.60
Sm	0.47	0.48	0.50	0.41	0.51	0.43	0.51	0.37	0.50	0.37	0.52	0.38	0.61	0.61	0.97	0.70
Eu	0.09	0.09	0.09	0.07	0.09	0.08	0.09	0.07	0.10	0.07	0.11	0.08	0.13	0.12	0.19	0.15
Gd	0.51	0.52	0.55	0.42	0.53	0.44	0.53	0.40	0.55	0.41	0.57	0.44	0.76	0.67	1.08	0.82
Tb	0.06	0.06	0.07	0.05	0.06	0.05	0.06	0.05	0.07	0.05	0.07	0.05	0.09	0.08	0.14	0.10
Dy	0.36	0.37	0.39	0.31	0.36	0.34	0.39	0.29	0.40	0.29	0.42	0.33	0.55	0.51	0.89	0.67
Ho	0.07	0.07	0.07	0.06	0.07	0.06	0.07	0.06	0.08	0.06	0.08	0.07	0.12	0.10	0.18	0.13
Er	0.19	0.19	0.20	0.16	0.19	0.18	0.20	0.16	0.22	0.15	0.23	0.18	0.32	0.28	0.51	0.36
Tm	0.03	0.03	0.02	0.02	0.03	0.02	0.02	0.02	0.03	0.02	0.03	0.02	0.04	0.04	0.07	0.05
Yb	0.15	0.16	0.15	0.13	0.15	0.13	0.16	0.13	0.16	0.11	0.18	0.14	0.24	0.21	0.39	0.28
Lu	0.02	0.02	0.02	0.02	0.02	0.02	0.02	0.02	0.02	0.02	0.03	0.02	0.04	0.03	0.06	0.05
∑REE	12.97	13.23	14.50	10.77	13.82	11.83	13.89	10.21	14.51	10.66	14.75	9.86	17.28	16.52	20.50	16.60
Nd_{SN}/Yb_{SN}	1.29	1.23	1.49	1.21	1.40	1.29	1.38	1.19	1.32	1.37	1.18	1.14	1.12	1.14	1.02	1.09
Ce/Ce*	1.08	1.09	1.14	1.19	1.11	1.15	1.08	1.10	1.07	1.17	1.06	0.89	0.96	1.06	0.40	0.49
log(Ce/Ce*)	0.03	0.04	0.06	0.08	0.05	0.06	0.03	0.04	0.03	0.07	0.02	-0.05	-0.02	0.03	-0.39	-0.31
Eu/Eu*	0.99	0.99	0.99	0.85	0.97	0.97	0.98	1.02	1.01	1.05	1.06	1.03	1.04	0.99	1.00	1.07
Gd/Gd*	1.39	1.37	1.36	1.37	1.37	1.31	1.33	1.29	1.33	1.34	1.30	1.35	1.38	1.34	1.27	1.31

Samples for REE and trace element analyses are prepared as follows. About 50 mg of powdered sample is weighed in Teflon beakers and leached by 1 M acetic acid in an ultrasonic bath for several hours to dissolve the carbonate fraction. After dissolution, the sample solutions are centrifuged and the supernatant transferred to clean Teflon beakers. The solutions are evaporated on a hotplate at 70–100 °C until dry. Finally, the samples are dissolved in 3% HNO_3 spiked with an internal Rh standard (10 ppb) for analysis. All the samples were analyzed by high resolution inductively coupled plasma mass spectrometer (HR-ICP-MS) at the State Key Laboratory for Mineral Deposits Research of Nanjing University. The analytical precision is estimated to be <10% according to duplicate analyses of samples and GSR-12 (GBW-07114, CAGS, a Chinese national rock standard).

4. Results

4.1. REE compositions

REE results of the Shenhu and Dongsha carbonates in the South China Sea are listed in Tables 3 and 4, respectively. Overall, the individual rare earth element concentrations of the Shenhu and Dongsha cold seep carbonates vary from 0.02 to 7.72 ppm, and 0.02 to 10.06 ppm, respectively, which lie within the range of average marine carbonates (0.04–14 ppm; Sarkar et al., 2003). The total REE concentrations of the Shenhu and Dongsha carbonates are mostly between 10 and 20 ppm, with average ∑REE values of 13.87 ppm and 15.54 ppm, respectively, which are low compared to the typical marine carbonate value of ~28 ppm reported by Bellanca et al. (1997).

REE concentrations were normalized to the Post-Achaean Australian Shale (PAAS) composite (McLennan, 1989). Shale-normalized elemental anomalies can be calculated as a ratio between the measured element concentration and the calculated concentration of that element derived from either a linear average or a geometric average of nearest-neighbor element concentrations. In most cases, the difference in the results obtained by these two methods is minor (<5%, Frimmel, 2009). In this study, anomalies are calculated as follows: $Ce/Ce^* = 3Ce/(2La + Nd)$, $Eu/Eu^* = 3Eu/(2Sm + Tb)$, $Gd/Gd^* = 2Gd/(Eu + Tb)$.

Previous studies have shown that Eu interferes with Ba during ICP-MS measurement (Dulski, 1994), often indicated by a good linear correlation between Ba/Sm and Eu/Eu* (Jiang et al., 2007). Such cases occur in phosphate nodules (Jiang et al., 2007) and barite (Hein et al., 2007). The

Table 4
REE concentrations (in ppm) for the Dongsha cold seep carbonates.

	TVG1	TVG2-C2	TVG3-C2	TVG13-B3	TVG14-C2 B	TVG14-C2 C	TVG14-C2 D	TVG14-C2 E	TVG14-C2 F	TVG14-C2 G	TVG6	TVG8-C1	TVG8-C4-2	TVG11-C2
La	3.66	4.81	3.21	3.76	2.77	2.41	2.18	2.30	2.89	2.63	5.14	3.71	4.81	2.34
Ce	6.16	5.07	4.84	5.58	5.65	4.75	4.21	4.25	5.01	4.46	8.75	8.46	10.06	4.99
Pr	0.79	1.00	0.66	0.73	0.62	0.53	0.47	0.50	0.61	0.56	1.05	0.84	1.06	0.49
Nd	3.06	3.78	2.52	2.83	2.25	1.97	1.72	1.83	2.34	2.11	3.92	2.99	3.80	1.80
Sm	0.63	0.78	0.43	0.56	0.49	0.43	0.36	0.36	0.47	0.43	0.78	0.64	0.82	0.35
Eu	0.13	0.16	0.08	0.12	0.10	0.09	0.08	0.08	0.10	0.09	0.16	0.13	0.18	0.07
Gd	0.96	1.11	0.54	0.85	0.63	0.56	0.52	0.59	0.69	0.64	1.16	0.85	1.16	0.49
Tb	0.12	0.14	0.07	0.11	0.08	0.07	0.07	0.07	0.09	0.08	0.15	0.11	0.15	0.06
Dy	0.71	0.84	0.39	0.65	0.52	0.48	0.44	0.47	0.59	0.54	0.91	0.66	0.95	0.37
Ho	0.14	0.17	0.07	0.13	0.11	0.09	0.09	0.10	0.12	0.12	0.19	0.14	0.19	0.07
Er	0.40	0.48	0.21	0.37	0.31	0.30	0.28	0.29	0.37	0.32	0.53	0.39	0.54	0.22
Tm	0.06	0.07	0.03	0.05	0.04	0.04	0.04	0.04	0.05	0.05	0.07	0.05	0.07	0.03
Yb	0.32	0.38	0.16	0.30	0.27	0.25	0.23	0.26	0.31	0.28	0.43	0.31	0.42	0.18
Lu	0.05	0.06	0.02	0.05	0.04	0.04	0.04	0.04	0.05	0.04	0.07	0.05	0.06	0.03
∑REE	17.19	18.85	13.21	16.10	13.88	12.00	10.71	11.19	13.71	12.36	23.28	19.33	24.27	11.51
Nd_{SN}/Yb_{SN}	0.80	0.86	1.38	0.80	0.71	0.66	0.65	0.61	0.64	0.64	0.78	0.82	0.77	0.85
Ce/Ce*	0.82	0.52	0.75	0.74	1.00	0.96	0.95	0.91	0.85	0.83	0.85	1.12	1.03	1.06
log(Ce/Ce*)	-0.09	-0.28	-0.13	-0.13	0.00	-0.02	-0.02	-0.04	-0.07	-0.08	-0.07	0.05	0.01	0.03
Eu/Eu*	0.99	0.97	0.93	0.97	1.03	1.03	1.01	1.04	0.98	1.01	0.93	0.97	1.00	0.96
Gd/Gd*	1.49	1.44	1.47	1.48	1.32	1.33	1.42	1.50	1.41	1.42	1.49	1.38	1.39	1.43

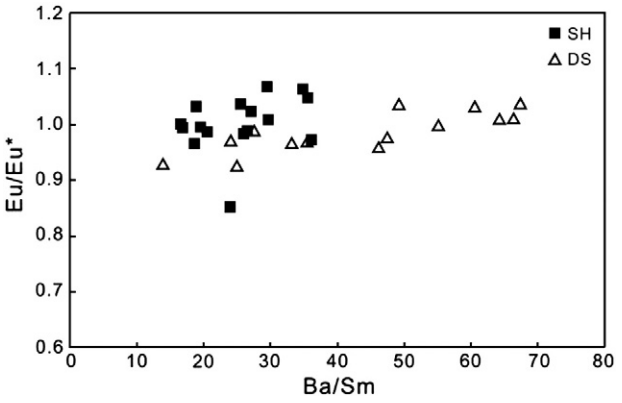

Fig. 3. Correlation between Eu/Eu* and Ba/Sm of the Shenhu and Dongsha cold seep carbonates.

lower Ba/Sm ratios and the lack of Ba/Sm and Eu/Eu* correlation in our samples (Fig. 3) suggest that the Eu anomalies are real and can be used as redox indicators. Eu/Eu* values of both Shenhu and Dongsha carbonates approach 1, indicating no obvious Eu anomaly in our studied samples (Tables 3 and 4).

The shale-normalized REE patterns of the Shenhu carbonates show the following characteristics: (1) slight light rare earth element (LREE) enrichment with Nd_{SN}/Yb_{SN} values of 1.02–1.49; (2) positive Ce anomaly in HS4DG-1 and HS4DG-2 samples (Ce/Ce* up to 1.19) and negative Ce anomaly in HS4DG-3 samples; and (3) a consistently positive Gd anomaly of 1.27–1.39 (Table 3; Fig. 4A–C). As a comparison, the typical features of the Dongsha carbonate REE patterns are: (1) slight heavy rare earth element (HREE) enrichment with Nd_{SN}/Yb_{SN} values of 0.61–0.86 (except one sample, 1.38); (2) variable Ce anomaly, mostly Ce/Ce*<1.0; and (3) more positive Gd anomaly (Gd/Gd* = 1.32–1.50) than the Shenhu samples (Gd/Gd* = 1.27–1.39).

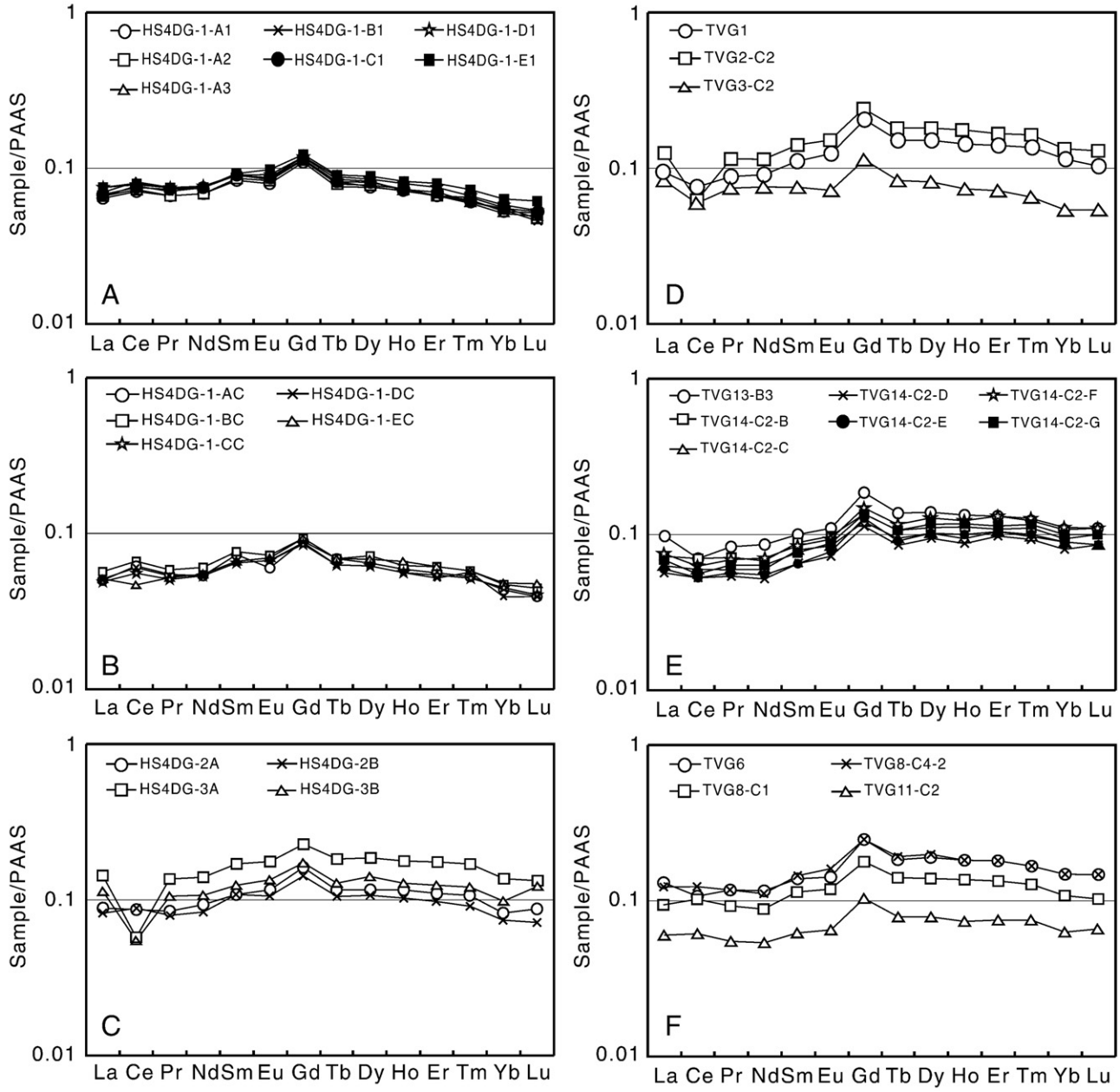

Fig. 4. Shale-normalized REE distribution patterns of the Shenhu and Dongsha cold seep carbonates. A-C show samples from the Shenhu area, and D-F present samples from three sites in Dongsha area.

4.2. Selected trace element compositions

Results of the selected trace elements, particularly the redox-sensitive trace elements, from both Shenhu and Dongsha cold seep carbonates are listed in Tables 5 and 6, respectively. In the Shenhu samples, Sr and Mn vary from 720 to 3640 and 643 to 1192 ppm, respectively. Concentrations of Ni, Zn, and Ba are also high and vary in the range of several tens of ppm. Concentrations of V, Cr, Mo, U, Sc, Ti, Co, Cu, Ga, Rb, Pb, and Th are in the sub-ppm to several ppm range (Table 5). We notice that concentrations of Co, Ni and U are higher than those of average marine carbonates (Turekian and Wedepohl, 1961). Concentrations of trace elements in Dongsha samples are somewhat higher than that of Shenhu samples, except for Mn and Sr (Table 6). Some elements show variable concentrations at different sites, such as Mo and U concentrations, which show an increase with water depth. The enrichment of Sr, with concentrations higher than normal marine carbonates (610 ppm), (Turekian and Wedepohl, 1961) is coincident with the presence of aragonite.

5. Discussion

5.1. REE system

Our studied cold seep carbonate samples from the Shenhu and Dongsha areas show low REE concentrations and low $\sum$REE values compared to normal marine carbonates (Sarkar et al., 2003), but are similar to the reported data of seep carbonates from SW Taiwan (Chen et al., 2005), the Gulf of Mexico (Feng et al., 2009b), and some ancient hydrocarbon-seep localities (Feng et al., 2009a). In shallow water environments on continental margins, fast sedimentation rates leave sediments exposed at or near the sediment-water interface for only a short period of time, which results in low concentrations of REE in biogenic apatite (Wright et al., 1987). Similarly, the REE content of seep carbonates is likely a function of precipitation rate, which is related to seepage rates. Slow seepage decreases the precipitation rate, kinetically favoring incorporation of REE and leading to high total REE concentrations. Conversely, when seepage is fast, carbonates will have limited time to incorporate REEs resulting in lower concentrations. The carbonate deposits displaying a chimney structure indicate that the fluid expulsion was relatively vigorous, or at least channelized (Saker et al., 2003). In this case, fast seepage may have caused low REE concentrations in our studied samples.

The shale-normalized REE pattern of modern seawater is characterized by a negative Ce anomaly, a positive La anomaly, and relative enrichment of the heavy rare earth elements (HREE) (Shields and Webb, 2004). Marine chemical sediments, which reflect seawater REE distribution independent of age, typically display a uniform light rare earth element (LREE) depletion, enrichment in La, depletion in Ce, as well as a slight enrichment in Gd in shale-normalized patterns (Frimmel, 2009). Shale-normalized REE patterns obtained from the Shenhu samples show slight LREE enrichment and a positive Ce anomaly (except for the HS4DG-3 samples; Fig. 4A–C), which does not conform to typical seawater patterns of marine chemical sediments. With respect to the Dongsha seep carbonates, many samples from sites 1 and 2 display REE patterns somewhat similar to marine chemical sediments, but samples from site 3 show a positive Ce anomaly (Fig. 4D–F). Authigenic carbonates are usually very well-preserved in hemipelagic or pelagic sediments (Feng et al., 2009a), and their REE patterns typically reflect the fluid characteristics from which they precipitated.

Previous studies reveal that $\delta^{18}O$ values of the Shenhu authigenic carbonate chimneys vary between +3.75‰ and +4.31‰ (Lu et al., 2006), while $\delta^{18}O$ of the Dongsha carbonates range from +1.7‰ to +5.3‰ (Han et al., 2008). Slightly heavy $\delta^{18}O$ values are interpreted to have precipitated from ^{18}O-rich hydrate-related fluids (cf. Bohrmann et al., 1998; Aloisi et al., 2002). Gas hydrate decomposition liberates ^{18}O-rich water which can contribute significantly to ^{18}O-enrichment of the interstitial solutions (Aloisi et al., 2002). The co-occurrence of authigenic carbonates in gas-hydrate sites indicates that carbonate formation may relate to the decomposition of the gas hydrates (Bohrmann et al., 1998; Aloisi et al., 2002).

We interpret the shale-normalized REE patterns of our samples to reflect the characteristics of the methane-enriched fluids from which they formed. Among them, samples from two sites (HS4DG-1 and HS4DG-2) in Shenhu and site 3 in Dongsha predominantly display the features of the original seepage fluids, or less importantly, the influence of other fluids such as surrounding pore water. These samples have slight LREE enrichment and positive Ce anomalies. One possibility for the source of methane-enriched fluids in the Shenhu carbonates likely relates to the decomposition of gas hydrates present at about 200 m depth below the seafloor (Zhang et al., 2007). However, samples from HS4DG-3 and sites 1 and 2 from the Dongsha area show a mixed signature of source fluids. These samples are likely to have significant influence of seawater (Han et al., 2008), which also indicates that these carbonates may have formed within sediments but near the seawater-sediment interface. Furthermore, the sediments at site 1146 of ODP 184 consist of carbonate-rich, hemipelagic nannofossil clays (Wang et al., 2000). The REE distribution pattern in the sediments reveals relative enrichment of LREE and a positive Ce anomaly (Liu et al., 2004). Hence, some contribution of clay dehydration to the source fluids cannot be excluded.

Table 5
Selected trace element concentrations (in ppm) for the Shenhu cold seep carbonates.

	HS4DG-1-A1	HS4DG-1-A2	HS4DG-1-A3	HS4DG-1-Ac	HS4DG-1-B1	HS4DG-1-Bc	HS4DG-1-C1	HS4DG-1-Cc	HS4DG-1-D1	HS4DG-1-Dc	HS4DG-1-E1	HS4DG-1-Ec	HS4DG-2-A	HS4DG-2-B	HS4DG-3-A	HS4DG-3-B
Sc	1.86	1.81	1.93	2.34	1.47	2.27	1.65	1.82	1.84	1.99	2.01	1.63	1.64	1.73	2.47	2.39
Ti	1.54	1.49	1.83	2.20	1.75	4.68	1.77	1.72	1.68	2.06	1.65	1.55	1.35	1.35	2.37	1.71
V	1.32	1.07	1.54	2.26	1.52	2.89	1.79	1.75	1.50	1.98	1.34	1.01	0.43	0.79	0.40	0.30
Cr	4.80	4.34	5.88	5.01	4.22	6.16	5.89	4.62	13.03	5.51	7.89	3.53	6.68	4.97	6.98	6.44
Mn	812	811	817	643	683	722	866	735	953	741	1111	697	1210	964	1992	1422
Co	1.42	1.16	1.92	2.37	1.37	3.24	1.80	1.75	2.38	2.92	2.89	1.06	2.01	1.87	2.08	1.63
Ni	25.33	23.00	26.14	32.72	22.93	30.60	25.19	29.73	30.08	27.59	30.35	31.98	22.08	22.31	55.64	37.94
Cu	1.14	0.92	1.53	1.59	1.30	1.46	1.35	1.27	1.54	1.21	1.44	1.32	0.82	0.85	2.52	1.57
Zn	6.88	6.13	7.93	6.93	6.11	8.99	7.53	6.43	284.08	7.45	13.06	9.55	17.85	16.83	17.21	15.68
Ga	0.76	0.74	0.76	0.63	0.62	0.68	0.74	0.64	0.86	0.72	1.01	0.64	1.08	0.92	1.55	1.13
Rb	2.96	2.36	3.73	2.94	2.27	4.50	3.87	2.87	4.58	3.60	7.59	2.15	6.05	4.06	4.73	5.36
Sr	1685	1447	1741	1370	1655	1290	1674	1665	1729	1554	1404	1645	720	827	3503	3640
Mo	0.09	0.07	0.11	0.18	0.11	0.20	0.11	0.20	0.31	0.19	0.11	0.12	0.08	0.07	0.15	0.35
Ba	9.59	8.09	13.27	9.77	9.41	15.57	13.18	10.17	14.95	13.00	17.95	7.16	15.72	11.81	15.98	20.72
Pb	0.58	0.56	0.71	0.61	0.76	1.21	0.63	0.35	0.64	0.84	1.44	0.38	1.14	1.36	0.37	2.02
Th	0.09	0.11	0.16	0.17	0.08	0.30	0.16	0.14	0.19	0.20	0.14	0.12	0.09	0.08	0.51	0.46
U	4.34	3.04	5.99	5.06	6.64	5.63	6.29	5.00	6.95	4.89	4.71	2.87	3.00	3.33	5.58	4.50

Table 6
Selected trace element concentrations (in ppm) for the Dongsha cold seep carbonates.

	TVG1	TVG2-C2	TVG3-C2	TVG13-B3	TVG14-C2 B	TVG14-C2 C	TVG14-C2 D	TVG14-C2 E	TVG14-C2 F	TVG14-C2 G	TVG6	TVG8-C1	TVG8-C4-2	TVG11-C2
Sc	241	3.10	2.65	2.88	3.23	3.42	3.41	3.80	3.70	4.69	3.39	3.38	3.22	3.19
Ti	1.96	2.08	2.82	2.09	3.58	4.53	4.25	4.16	4.82	6.26	2.62	4.29	2.38	4.09
V	1.29	0.40	0.73	0.99	7.41	5.65	7.25	8.78	7.63	9.18	2.49	12.99	8.38	10.44
Cr	5.08	5.79	3.70	14.11	7.43	7.44	6.87	7.55	7.45	9.48	6.38	7.54	6.97	5.93
Mn	1051	1180	308	1338	351	342	326	261	376	416	534	230	204	131
Co	2.11	2.40	6.80	6.11	3.36	3.30	2.90	3.44	3.80	5.05	9.01	3.54	2.46	2.59
Ni	27.12	40.71	31.02	38.61	33.08	36.76	36.63	38.78	38.70	44.55	33.56	28.02	26.99	31.55
Cu	1.80	4.16	1.51	1.90	2.43	2.53	2.17	2.40	2.14	2.73	2.62	0.77	0.82	0.62
Zn	18.05	28.78	9.64	197.57	22.61	18.93	18.52	19.94	19.09	25.38	16.39	20.36	26.35	85.05
Ga	1.37	1.59	0.86	1.69	0.66	0.71	0.63	0.65	0.78	0.94	1.31	0.95	1.07	0.62
Rb	3.88	5.10	2.14	6.02	6.45	7.03	5.24	5.93	5.58	7.50	2.97	5.29	6.23	5.80
Sr	430	1383	4629	620	929	1093	1100	1111	1041	1013	1173	701	561	3184
Mo	0.16	0.10	0.08	0.38	0.08	0.12	0.11	0.24	0.14	0.16	0.10	3.00	1.61	3.23
Ba	17.42	18.88	10.67	20.00	23.99	26.22	23.41	24.46	22.50	28.40	10.86	21.43	45.56	16.22
Pb	0.55	0.70	2.92	1.33	2.29	1.33	1.08	1.17	1.37	1.95	2.51	2.26	2.57	0.80
Th	0.11	0.41	0.42	0.14	0.48	0.30	0.26	0.25	0.34	0.36	0.61	0.74	0.77	0.57
U	2.47	3.06	2.36	2.38	0.98	0.91	0.97	1.11	2.02	2.59	9.22	15.93	11.65	11.07

Positive Gd anomalies have been described from both seawater and river waters (Lawrence et al., 2006). Consequently, the positive Gd anomalies in all the samples are not considered particularly diagnostic of a specific depositional environment (see Frimmel, 2009). Although samples from both Shenhu and Dongsha display no obvious Eu anomalies, it at least suggests that no strongly oxic conditions occurred during their precipitation (Jiang et al., 2007).

5.2. Ce anomaly

Variations in Ce are likely controlled by redox reactions, because Ce has two possible oxidation states, Ce^{3+} and Ce^{4+}. The removal of Ce from seawater takes place due to oxidation of soluble Ce^{3+} to insoluble Ce^{4+} (Wright et al., 1987; Sarkar et al., 2003). Marine limestones precipitating from such oxygenated seawater reflect this pattern, showing a negative Ce anomaly. However, under anoxic conditions, Ce remains soluble, and the precipitating calcites are characterized by a normal or sometimes elevated concentration of Ce, and consequently, they may display positive Ce anomalies (Sarkar et al., 2003). Thus, Ce is a sensitive indicator of redox precipitation conditions. Because diffusion or advection influences the distribution of redox sensitive species, it is likely that a gradient in redox conditions can exist (Wright et al., 1987). The reference point where no Ce anomaly is present, i.e. the Ce anomaly division between oxic and anoxic conditions, is set at -0.10, as suggested by Elderfield and Pagett (1986) and Wright et al. (1987).

In the diagram of Ce anomaly *vs.* Nd concentrations (Fig. 5), most of our studied samples plot near or above the anoxic–oxic boundary, indicating that these carbonates may have formed in anoxic conditions.

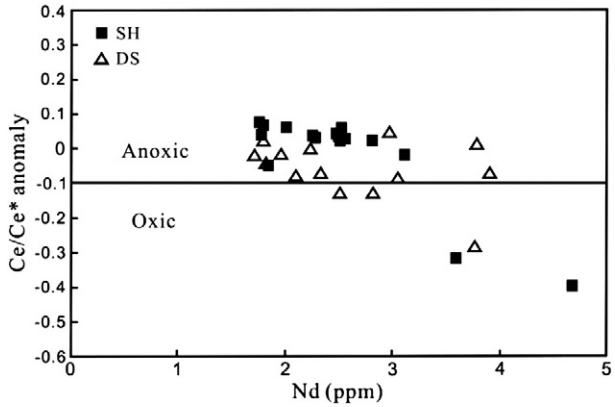

Fig. 5. Plot of Ce/Ce* anomaly *vs.* Nd concentration of the Shenhu and Dongsha cold seep carbonates. Ce/Ce* anomaly = log (Ce/Ce*).

The carbonate chimneys were sampled at the seafloor above/near the sediment surface, but since they incorporate many terrigenous components, these chimneys should have initially formed within the unconsolidated sediments, and later became exposed by erosion (similar to the cases reported by Stakes et al., 1999 and Peckmann et al., 1999). The HS4DG-1 chimney in the Shenhu area shows a gradient rare earth element variation from rim to core, with Ce anomaly values (Ce/Ce*) of the rim being slightly lower than that of the core (except sample E, see Table 3). We consider that this may record a two-stage seepage during the formation of the chimney, which is consistent with C isotope evidence (Lu et al., 2006). During an early stage, the rim of the chimney firstly formed in an anoxic environment in the sediments, with a positive Ce anomaly. During the subsequent seepage, carbonates precipitated in core channels of the chimney, which was likely a semi-isolated environment, resulting in an even more anoxic condition, and therefore showing a higher positive Ce anomaly. However, there is one exception for samples at site HS4DG-3, which show negative Ce anomalies (0.40 and 0.49), suggesting that this chimney may have formed in a more oxygen-rich depositional setting. The differences of two stages for the formation of these chimneys may be a result of changing seepage conditions, e.g., the fluid sources, speed of seepage, and characteristics of fluids.

In the Dongsha area, Ce anomaly values of seep carbonates show an increase with water depth (Fig. 6). Seep carbonates from sites 1 and 2 possess a brownish Fe–Mn coating, indicating that they may have been exposed to bottom water for some time (Han et al., 2008). Weathering of carbonates may have changed the primary Ce signature. This is one possibility, but according to the REE system, carbonates at these two sites reveal a mixed fluid source. That is, the original seepage was influenced by seawater. Oxygen concentrations in the water column from the Dongsha area slightly decreased with water depth and the oxygen minimum zone there is between 700 and 900 m (Suess, 2005). It is more likely that seawater also brought some oxygen into the original anoxic seepage resulting in Ce anomaly values (log Ce/Ce*) varying between -0.29 and 0.00. Although Ce anomalies show oxic signatures, we stress that carbonates formed in predominantly anoxic conditions may locally include a small amount of oxygen. Site 3 has negligible influence of other fluids, and it is characterized by an anoxic Ce anomaly (Fig. 6). The site 3 cold seep system may still be active, as indicated by slightly elevated methane concentrations in the bottom water (Suess, 2005) and the presence of bacterial linings (Han et al., 2008). This is coincident with the environment becoming more anoxic with increasing water depths.

5.3. Trace elements

Previous studies have indicated that some trace elements, such as Mo, U, Ni, V, Cr, Co, and Zn, are redox sensitive metals in marine sediments

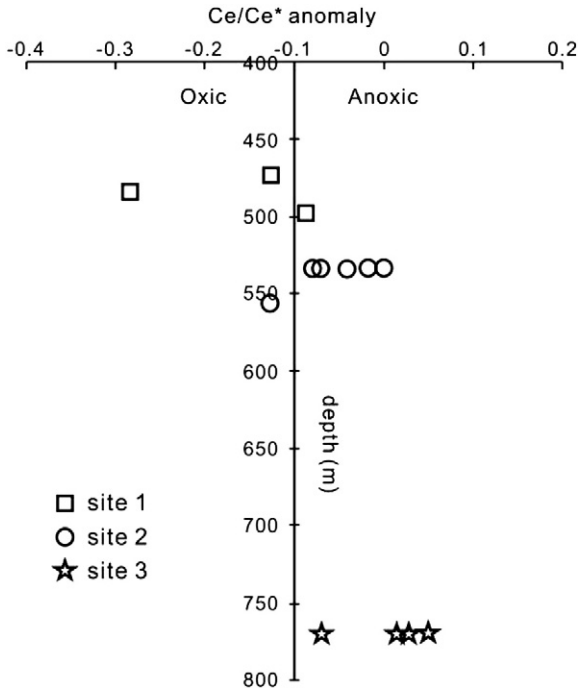

Fig. 6. Profiles of Ce/Ce* anomaly of the Dongsha seep carbonates varying with water depths.

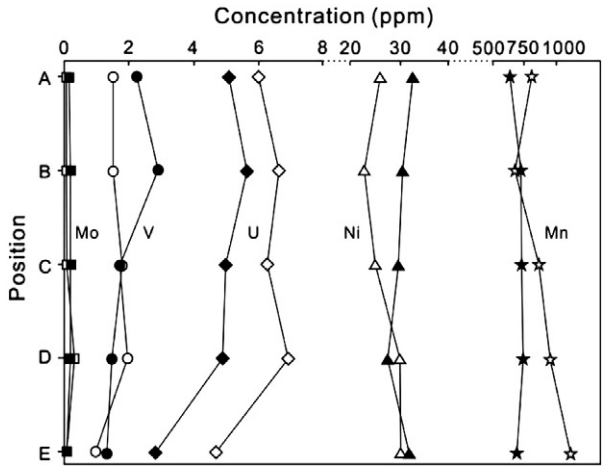

Fig. 7. Redox-sensitive element variation of HS4DG-1 chimney from the rim to core. The position of A–E is marked in Fig. 2A. Solid symbols represent the core and open symbols represent the rim.

(Jacobs et al., 1985; Dean et al., 1997; Morford and Emerson, 1999; Sarkar et al., 2003), whereby enrichment of these elements is the result of preferential concentration in anoxic conditions. Mo concentration has been found to be considerably higher in settings where free H_2S is present. When MoO_4^{2-} changes to MoS_4^{2-} as HS^- increases, Mo is removed from anoxic seawater (Sarkar et al., 2003). Similarly, under oxygen-deficient/reducing condition, U^{6+} is reduced to its immobile U^{4+} state (Klinkhammer and Palmer, 1991). Apart from Mo and U, V can also act as a palaeo-redox indicator (Sarkar et al., 2003). Anoxic sediment is a sink for marine V, making it a potential tool to determine redox conditions (Breit and Wanty, 1991). In the absence of oxygen, $H_2VO_4^-$ is reduced to V (IV)O^{2+}, and binds even more strongly to chelating surface groups than the larger anionic $H_2VO_4^-$ (Morford and Emerson, 1999). Enrichment of other trace metals like Ni, Co, and Zn are found at elevated concentrations in laminated anoxic conditions (Jacobs et al., 1985; Dean et al., 1997).

In this study, the concentrations of U, Ni and Co in both the Shenhu and Dongsha samples are higher than average marine carbonate values (U = 2.2 ppm; Ni = 20 ppm; Co = 0.1 ppm; Turekian and Wedepohl, 1961). The high concentrations of these trace elements are thought to reflect reducing conditions during carbonate precipitation. The chimney from the Shenhu area shows an increase in Mo, V, and Ni from the rim to core, while the concentrations of U and Mn decrease from the rim to core (Fig. 7). The increase in the redox sensitive elements likely records the changing precipitation conditions during chimney growth, and indicates more anoxic conditions, which is consistent with the reported changes in Ce anomaly. The chimneys show two stages of seepage, with a more anoxic fluid during core formation. In this case, the redox sensitive metal concentrations of the core are higher than the rim. Because anoxic and reducing conditions produce soluble Mn^{2+}, the decrease of Mn content from the rim to core may indicate progressively more reducing precipitation conditions (Jiang et al., 2007). In the Dongsha area, V, Mo and U concentrations also show an increase with water depths (Fig. 8), concording with the recorded variation in Ce anomaly, all these data indicating that site 3 is more anoxic than sites 1 and 2 at Dongsha.

5.4. Environment of cold seep carbonate precipitation

It is widely accepted that seep carbonates are products of anaerobic oxidation of methane (Hinrichs et al., 1999). However, there is growing evidence for aerobic methanotrophy at seep sites (Feng et al., 2009a). Carbonates from the Shenhu area are mainly composed of dolomite (Table 2). Dolomite precipitation is favored when dissolved sulfate is absent or present at very low concentrations (Aloisi et al., 2000). The Shenhu chimneys may have deposited around sulfate/methane interface in the sediments, where sulfate was depleted. This anoxic condition resulted in positive Ce anomalies and the enrichment of redox sensitive trace elements in the carbonates. Two stages of seepage are recognized during the formation of chimneys, which have different speed and fluxes of seepage.

Carbonates from the Dongsha area are predominantly aragonite and high magnesium calcite (Table 2). The formation of these minerals are favored at high SO_4^{2-} concentrations and Mg^{2+}/Ca^{2+} ratios (Aloisi et al., 2000). Conditions similar to these should be met at the uppermost part of the sediments. When methane-enriched fluids migrate upward to this zone, the small downward flux of oxic seawater entering the anoxic sediments is insufficient to entirely

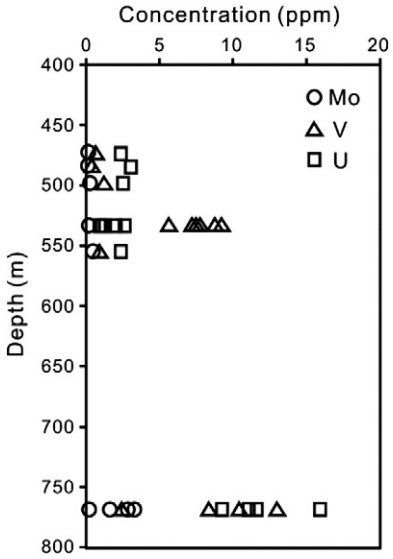

Fig. 8. Profiles of concentrations of redox-sensitive elements Mo, V and U of the Dongsha seep carbonates varying with water depths.

change the depositional conditions from anoxic to oxic in the shallow sediments (e.g. Feng et al., 2009a). The REE patterns of carbonate precipitates in this zone should show some seawater influence, with slight HREE enrichment and no or negative Ce anomalies. Seawater may locally include a small amount of oxygen into the fluids. Carbonates formed in this condition will show some negative Ce anomalies. Lipid biomarkers of seep carbonates from the Dongsha area document the existence of an anaerobic oxidation of methane (Yu et al., 2008).

6. Conclusions

1) Cold seep carbonates were sampled from two areas (Shenhu and Dongsha) on the northern continental slope of the South China Sea. Their geochemical characteristics, with low REE concentrations, atypical seawater-like shale-normalized REE patterns, consistently positive Gd anomalies, enrichment in redox sensitive trace elements, and varied Ce anomalies, reflect the characteristics of source fluids and chemical conditions during precipitation.

2) Positive Ce anomalies and concentrations of redox sensitive trace elements, such as Mo, U, Ni, V, and Mn in the Shenhu cold seep carbonate chimneys increase from the rim to core. This may be the result of variable seepage conditions, with more anoxic conditions during the core formation stage. Carbonates from the HS4DG-3 site, with negative Ce anomalies, may precipitate from fluids which are impacted by surrounding sediments.

3) The typical features of the REE patterns and redox sensitive trace elements in the Dongsha samples reveal less/more anoxic conditions for the formation of these cold seep carbonates. Furthermore, concentrations of some trace elements show an increase with water depth, which is coincident with the observed change in Ce anomaly values. The source fluids of the Dongsha carbonates, with slight enrichment of HREE and redox sensitive trace elements, a more positive Gd anomaly and negative Ce anomalies, have likely been influenced by seawater.

Acknowledgments

Funding for this research was provided by National Science Foundation of China (grant no. 40773029) and a National 973 Project (grant no. 2009CB219506). The manuscript benefited from thoughtful suggestions by N. Gary Hemming, and three anonymous reviewers.

References

Aloisi, G., Pierre, C., Rouchy, J.M., Faugeres, J.C., Woodside, J., The MEDINAUT Scientific Party, 2000. Methane-related authigenic carbonates of eastern Mediterranean Sea mud volcanoes and their possible relation to gas hydrate destabilisation. Earth and Planetary Science Letters 184, 321–338.

Aloisi, G., Pierre, C., Rouchy, J.M., Faugeres, J.C., 2002. Isotopic evidence of methane-related diagenesis in the mud volcanic sediments of the Barbados Accretionary Prism. Continental Shelf Research 22, 2355–2372.

Bellanca, A., Muetti, D., Neri, R., 1997. Rare earth elements in limestone/mudstone couplets from the Albian–Cenomanian Cismon section (Venctian region, north Italy): assessing REE sensitivity to environmental changes. Chemical Geology 141, 141–152.

Bohrmann, G., Greinert, J., Suess, E., Torres, M., 1998. Authigenic carbonates from the Cascadia subduction zone and their relation to gas hydrate stability. Geology 26, 647–650.

Breit, G.N., Wanty, R.B., 1991. Vanadium accumulation in carbonaceous rocks: a review of geochemical controls during deposition and diagenesis. Chemical Geology 91, 83–97.

Campbell, K.A., Farmer, J.D., Marais, D.D., 2002. Ancient hydrocarbon seeps from the Mesozoic convergent margin of California: carbonate geochemistry, fluids, and palaeoenvironments. Geofluids 2, 63–94.

Canet, C., Prol-Ledesema, R.M., Melgarejo, J.C., Reyes, A., 2003. Methane-related carbonates formed at submarine hydrothermal springs: a new setting for microbially-derived carbonates? Marine Geology 199, 245–261.

Chen, D.F., Huang, Y.Y., Yuan, X.L., Cathles III, L.M., 2005. Seep carbonates and preserved methane oxidizing archaea and sulfate reducing bacteria fossils suggest recent gas venting on the seafloor in the Northeastern South China Sea. Marine and Petroleum Geology 22, 613–621.

D'Hondt, S., Rutherford, S., Spivack, A.J., 2002. Metabolic activity of subsurface life in deep-sea sediments. Science 295, 2067–2070.

Dean, W.F., Gardner, J.V., Piper, D.Z., 1997. Inorganic geochemical indicators of glacial–interglacial changes in productivity and anoxia on the California continental margin. Geochimica et Cosmochimica Acta 61, 4507–4518.

Dulski, P., 1994. Interferences of oxide, hydroxide and chloride analyte species in the determination of rare earth elements in geological samples by inductively coupled plasma-mass spectrometry. Fresenius' Journal of Analytical Chemistry 350, 194–203.

Elderfield, H., Pagett, R., 1986. REE in Ichthyoliths: variation with redox conditions and depositional environment. Science of the Total Environment 49, 175–197.

Feng, D., Chen, D.F., 2008. Petrographic characterization and rare earth elements as geochemical tracers for redox condition of seep carbonates from northwestern Black Sea. Geoscience 22, 390–396 (in Chinese with English abstract).

Feng, D., Chen, D.F., Peckmann, J., 2009a. Rare earth elements in seep carbonates as tracers of variable redox conditions at ancient hydrocarbon seeps. Terra Nova 21, 49–56.

Feng, D., Chen, D.F., Roberts, H.H., 2009b. Petrographic and geochemical characterization of seep carbonate from Bush Hill (GC 185) gas vent and hydrate site of the Gulf of Mexico. Marine and Petroleum Geology 26, 1190–1198.

Feng, D., Chen, D.F., Peckmann, J., Bohrmann, G., 2010. Authigenic carbonates from methane seeps of the northern Congo fan: microbial formation mechanism. Marine and Petroleum Geology 27, 748–756.

Frimmel, H.E., 2009. Trace element distribution in Neoproterozoic carbonates as palaeoenvironmental indicator. Chemical Geology 258, 338–353.

Haley, B.A., Klinkhammer, G.P., Mcmanus, J., 2004. Rare earth elements in pore waters of marine sediments. Geochimica et Cosmochimica Acta 68, 1265–1279.

Han, X.Q., Suess, E., Huang, Y.Y., Wu, N.Y., Bohrmann, G., Su, X., Eisenhauer, A., Rehder, G., Fang, Y.X., 2008. Jiulong methane reef: microbial mediation of seep carbonates in the South China Sea. Marine Geology 249, 243–256.

Hein, J.R., Zierenberg, R.A., Barry Maynard, J., Hannington, M.D., 2007. Barite-forming environments along a rifted continental margin, Southern California Borderland. Deep-Sea Research II 54, 1327–1349.

Hinrichs, K.U., Hayes, J.M., Sylva, S.P., Brewer, P.G., Delong, E.F., 1999. Methane-consuming archaebacteria in marine sediments. Nature 398, 802–805.

Jacobs, L., Emerson, S., Skei, J., 1985. Partitioning and transport of metals across the O_2/H_2S interface in a permanently anoxic basin: Framvaren Fjord, Norway. Geochimica et Cosmochimica Acta 49, 1433–1444.

Jiang, S.Y., Yang, J.H., Ling, H.F., Yang, T., Chen, D.F., Xue, Z.C., Ji, J.F., Ni, P., 2004. Search for gas hydrates in the South China Sea: a geochemical approach. Marine Geology & Quarternary Geology 24, 103–109.

Jiang, S.Y., Zhao, H.X., Chen, Y.Q., Yang, T., Yang, J.H., Ling, H.F., 2007. Trace and rare earth element geochemistry of phosphate nodules from the lower Cambrian black shale sequence in the Mufu Mountain of Nanjing, Jiangsu province, China. Chemical Geology 244, 584–604.

Jin, C., Wang, J., 2002. Preliminary study on the gas hydrates stability zone in the South China Sea. Acta Geologica Sinica 76, 423–428 (in Chinese with English abstract).

Klinkhammer, G.P., Palmer, M.R., 1991. Uranium in the oceans, where it goes and why. Geochimica et Cosmochimica Acta 55, 1799–1806.

Kruger, M., Treude, Y., Wolters, H., Nauhaus, K., Boetius, A., 2005. Microbial methane turnover in different marine habitats. Palaeogeography, Palaeoclimatology, Palaeoecology 227, 6–17.

LaRock, P.A., Hyun, J.H., Bennison, B.W., 1994. Bacterioplankton growth and production at the Louisiana hydrocarbon seeps. Geo-Marine Letters 14, 104–109.

Lawrence, M.G., Greig, A., Collerson, K.D., Kamber, B.S., 2006. Rare earth element and yttrium variability in South East Queensland waterways. Aquatic Geochemistry 12, 39–72.

Liu, B.L., Wang, Y.P., Wang, J.Z., Li, J.P., Wang, Y.H., Cheng, D.W., Li, Y., 2004. Geochemical characters of REE in the seafloor sediment in northern continental slope of the South China Sea and analysis of source of material and diagenesis environment. Marine Geology & Quaternary Geology 24, 17–23 (in Chinese with English abstract).

Lu, H.F., Chen, F., Liu, J., Liao, Z.L., Sun, X.M., Su, X., 2006. Characteristics of authigenic carbonate chimneys in Shenhu area, northern South China Sea: recorders of hydrocarbon-enriched fluid activity. Geological Review 52, 352–357 (in Chinese with English abstract).

McDonnell, S.L., Max, M.D., Cherkis, N.Z., Czarnecki, M.F., 2002. Tectono-sedimentary controls on the likelihood of gas hydrate occurrence near Taiwan. Marine and Petroleum Geology 17, 929–936.

McLennan, S.M., 1989. Rare earth elements in sedimentary rocks; influence of provenance and sedimentary processes. Reviews in Mineralogy and Geochemistry 21, 169–200.

Morford, J.L., Emerson, S., 1999. The geochemistry of redox sensitive trace metals in sediments. Geochimica et Cosmochimica Acta 63, 1735–1750.

Paull, C.K., Chanton, J.P., Neumann, A.C., Coston, J.A., Martens, C.S., Showers, W., 1992. Indicators of methane-derived carbonates and chemosynthetic organic carbon deposits: examples from the Florida Escarpment. Palaios 7, 361–375.

Peckmann, J., Thiel, V., 2004. Carbon cycling at ancient methane-seeps. Chemical Geology 205, 443–467.

Peckmann, J., Theil, V., Michaelis, W., Clari, P., Gaillard, C., Martire, L., Reitner, J., 1999. Cold seep deposits of Beauvoisin (Oxfordian; Southeastern France) and Marmorito (Miocene; northern Italy): microbially induced authigenic carbonates. International Journal of Earth Sciences 88, 60–75.

Peckmann, J., Reimer, A., Luth, U., Luth, C., Hansen, B.T., Heinicke, C., Hoefs, J., Reitner, J., 2001. Methane-derived carbonates and authigenic pyrite from the northwestern Black Sea. Marine Geology 177, 129–150.

Reeburgh, W.S., 1976. Methane consumption in Carian Trench waters and sediments. Earth and Planetary Science Letters 28, 337–344.
Ritger, S., Carson, B., Suess, E., 1987. Methane-derived authigenic carbonates formed by subduction-induced pore-water expulsion along the Oregon/Washington margin. Geological Society of America Bulletin 98, 147–156.
Sarkar, A., Sarangi, S., Ebihara, M., Bhattacharya, S.K., Ray, A.K., 2003. Carbonate geochemistry across the Eocene/Oligocene boundary of Kutch, western India: implications to oceanic O_2-poor condition and foraminiferal extinction. Chemical Geology 201, 281–293.
Shields, G.A., Webb, G.E., 2004. Has the REE composition of seawater changed over geological time? Chemical Geology 204, 103–107.
Shyu, C.T., Hsu, S.K., Liu, C.S., 1998. Heat flows off southwest Taiwan: measurements over mud diapirs and estimated from bottom simulating reflectors. Terrestrial Atmospheric and Oceanic Sciences 9, 795–812.
Stakes, D.S., Orange, D., Paduan, J.B., Salamy, K.A., Maher, N., 1999. Cold-seeps and authigenic carbonate formation in Monterey Bay, California. Marine Geology 159, 93–109.
Suess, E., 2005. RV SONNE cruise report SO 177, Sino–German cooperative project, South China Sea Continental Margin: geological methane budget and environmental effects of methane emissions and gas hydrates. IFM-GEOMAR Reports. http://store.pangaea.de/documentation/Reports/SO177.pdf.
Turekian, K.L., Wedepohl, K.H., 1961. Distribution of elements in some major units of the earth's crust. Geological Society of America Bulletin 72, 175–192.
Wallmann, K., Linke, P., Suess, E., Bohrmann, G., Sahling, H., Schluter, M., Dahlmann, A., Lammers, S., Greinert, J., von Mirbach, N., 1997. Quantifying fluid flow, solute mixing, and biogeochemical turnover at cold vents of the eastern Aleutian subduction zone. Geochimica et Cosmochimica Acta 61, 5209–5219.
Wang, P., Prell, W.L., Blum, P., 2000. Proceedings of ODP, Initial Report., 184: College Station, TX (Ocean Drilling Program).
Webb, G.E., Kamber, B.S., 2000. Rare earth elements in Holocene reefal microbialites: a new shallow seawater proxy. Geochimica et Cosmochimica Acta 64, 1557–1565.
Wright, J., Schrader, H., Holser, W.T., 1987. Paleoredox variations in ancient oceans recorded by rare earth elements in fossil apatite. Geochimica et Cosmochimica Acta 51, 631–644.
Wu, N., Suess, E., Jiang, H., Fu, S., Domeyer, B., Huang, Y., Zhu, Y., 2006. Pore-water geochemistry of surface sediments from Haiyang 4 area of the northeastern South China Sea. 2006 Western Pacific Geophysics Meeting: EOS Trans. AGU abstract, 87, pp. OS31A–0098.
Yu, X.G., Han, X.Q., Li, H.L., Jin, X.B., Gong, J.M., Suess, E., Huang, Y.Y., Wu, N.Y., Su, X., 2008. Biomarkers and carbon isotope composition of anaerobic oxidation of methane in sediments and carbonates of northeastern part of Dongsha, South China Sea. Acta Oceanologica Sinica 30, 77–84 (in Chinese with English abstract).
Zhang, H., Yang, S., Wu, N., Schultheiss, P., GMGS-1 science team, 2007. China's first gas hydrate expedition successful. Fire in the Ice: Methane Hydrate Newsletter, National Energy Technology Laboratory. U.S. Department of Energy. Spring/Summer issue, 1.